Computation of the crack opening displacements for Vickers indentation cracks

T. Fett

Institut für Materialforschung

Computation of the crack opening displacements for Vickers indentation cracks

Abstract:

Vickers indentation cracks are an appropriate tool to determine the crack-tip toughness K_{I0} and possibly the bridging relation of ceramics with an R-curve behaviour from the total crack opening displacements. Two contributions to the total crack opening displacement field are addressed. First, the residual stresses occurring in the uncracked body are considered and then, the contact stresses generated by preventing crack-face penetration are computed. The COD solution resulting from superposition of residual and contact displacements is given in the form of diagrams for graphic interpolation and in the form of a table for interpolation by bi-cubic splines. In addition, an analytical expression is provided. The near-tip displacements are represented by the first terms of series expansions.

Berechnung des Rissuferverschiebungsfelds für Vickerseindruckrisse

Kurzfassung:

Die beim Vickers-Eindruckversuch in keramischen Materialien auftretenden Risse sind geeignet, die Rissspitzenzähigkeit K_{I0} und möglicherweise auch die Brückenspannungen von Keramiken mit R-Kurveneffekt aus Rissuferverschiebungsmessungen zu bestimmen. Es werden zwei verschiedene Beiträge zur Rissuferverschiebung angesprochen. Zum einen ist das beim Eindruck in der ungerissenen Probe entstehende Eigenspannungsfeld für einen Teil der Verschiebungen in der gerissenen Probe verantwortlich. Andererseits ist auch das Spannungs- und Verschiebungsfeld erforderlich, das durch Kontaktspannungen im inneren Rissbereich auftritt. Die Gesamtverschiebungen resultieren aus der Überlagerung dieser beiden Beiträge. Die Ergebnisse der Berechnungen werden in Form von Diagrammen für graphische Interpolation und einer Tabelle für Spline-Interpolation wieder gegeben. Zusätzlich werden Näherungsformeln für das Gesamt- und das Rissspitzen-Nahfeld hergeleitet.

Contents

1. Introduction

The increasing crack resistance of ceramic materials is often caused by crack-bridging effects occurring between the opened crack surfaces. For the determination of bridging stresses for cracks in ceramic materials, it is necessary to know the crack opening profile in the absence of any bridging effect, the "applied" crack opening displacements δ_{appl} caused by the externally applied load. The differences between the applied and the measured total displacements (δ_{total}) are called "bridging displacements" δ_{br}, i.e. $\delta_{br} = \delta_{total} - \delta_{appl}$ with $\delta_{br} < 0$. From the difference between the applied and the measured displacements, the bridging stresses σ_{br} can be determined by solving an integral equation (see e.g. [1]).

In the case of fracture mechanics test specimens, the applied displacements can be computed from the externally applied load. In the case of a Vickers indentation, the residual stress field caused by non-elastic deformations is responsible for the applied displacements. A few studies were performed in the past to compute these displacements from the residual stresses (e.g. [2]). The main problem in the evaluation is how to deal with negative displacement in the damage zone.

It is the aim of this report to compute the "applied" crack opening displacement field caused by a superposition of residual stresses in the uncracked material, which result from Vickers indentation and contact stresses in the inner contact zone. For this purpose, the indentation crack is assumed to be semi-circular. It is furthermore assumed that the crack can be described as a half of a fully embedded crack, i.e. a change of the stress intensity factor along the crack contour is neglected.

2. Residual stress intensity factor and COD

2.1 Residual stresses

For the description of the residual stress field in the uncracked body, the model of an internally pressurised cavity [3,4] is applied. This model yields for the tangential component of residual stresses

$$\sigma_{res} = \begin{cases} -p\,f(r/b) & \text{for } r < b \\ C\,p\,(b/r)^3 & \text{for } r > b \end{cases} \tag{1}$$

with the coefficient C resulting from the equilibrium condition as

$$C = \frac{1}{b^2} \int_0^b f(r/b)\,r\,dr \tag{2}$$

For the geometric data see Fig. 1. The stress distribution according to eqs.(1) and (2) is illustrated in Fig. 2 for the case of $f(r/b) = 1$.
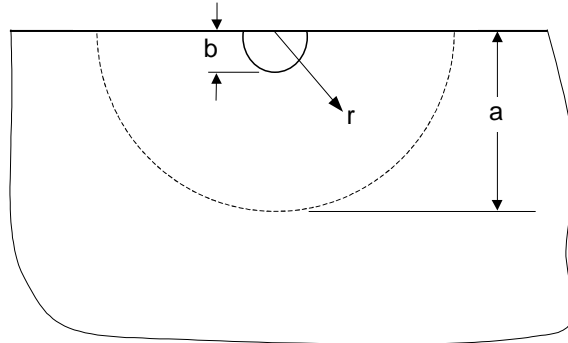

Fig. 1 Deformation zone and geometrical quantities.

2.2 Residual stress intensity factor

The residual stress intensity factor for a crack of radius a is given as

$$K_{res} = \frac{2}{\sqrt{\pi a}} \int_0^a \frac{r\,\sigma_{res}(r)\,dr}{\sqrt{a^2 - r^2}} \tag{3a}$$

or

$$K_{res} = -\frac{2}{\sqrt{\pi a}} \int_0^b \frac{r\,p\,f(r/b)\,dr}{\sqrt{a^2 - r^2}} + \frac{2C\,p}{\sqrt{\pi a}} \left(\frac{b}{a}\right)^2 \sqrt{a^2 - b^2} \tag{3b}$$
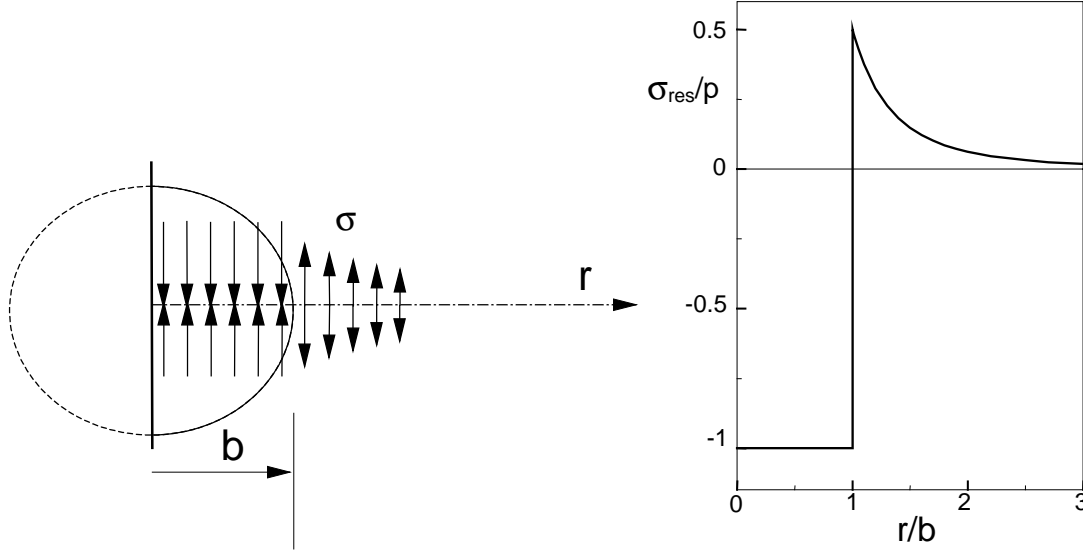
Fig. 2 Residual stress distribution in the absence of a crack according to eq.(1) for $f(r/b) = 1$.

It can be shown that the residual stress intensity factor is negative for any function $f(r/b)$ and any crack size a. Application of the mean value theorem to the first term of eq.(3b) with eq.(2) yields

$$-\frac{2}{\sqrt{\pi a}}\int_0^b \frac{r\, p\, f(r/b)\, dr}{\sqrt{a^2-r^2}} = -\frac{2p}{\sqrt{\pi a}}\frac{1}{\sqrt{a^2-r_0^2}}\int_0^b r\, f(r/b)\, dr \xrightarrow{\ eq.(2)\ } = -\frac{2C\, p}{\sqrt{\pi a}}\frac{b^2}{\sqrt{a^2-r_0^2}}$$

with a certain radius $0 \le r_0 \le b$.

$$K_{res} = -\frac{2C\, pb^2}{a^{3/2}\sqrt{\pi}}\left(\frac{1}{\sqrt{1-(r_0/a)^2}} - \sqrt{1-(b/a)^2}\right) \le 0 \qquad (4)$$

since the bracket is positive for any r_0 and b. As a first consequence of the negative residual stress intensity factor, penetration of the crack faces has to be expected at least for the near-tip crack opening displacement field.

2.3 Displacements caused by the residual stresses

In order to demonstrate the penetration of crack faces in the residual stress field, the crack opening displacements δ have to be computed. It holds

$$\delta_{res}(r) = \frac{4}{\pi E'}\int_r^a \left(\int_0^{a'}\frac{r'\sigma_{res}(r')}{\sqrt{a'^2-r'^2}}dr'\right)\frac{da'}{\sqrt{a'^2-r^2}} \qquad (5)$$

with the Young's modulus for plane strain E'. For a simpler representation of results, the stress intensity factors and crack opening displacements are normalised as

$$\delta' = \frac{\pi E'}{4pb}\delta, \quad K' = \frac{K}{p\sqrt{b}} \qquad (6)$$

3

Figure 3 shows the crack opening displacements δ_{res} for homogeneous p, i.e. for $f(r/b) = 1$.

The displacements (Figs. 3a and 3b) are negative over the whole crack area, and crack-face penetration occurs at any distance r/a. A decomposition of the displacements is given in Fig. 3c. Curve 2) was computed from the compressive stresses in $r < b$ exclusively and for curve 3) only the positive residual stresses at $r > b$ were considered. It is of importance to know that stresses active outside $r = b$ will affect the COD also in the region $r < b$.
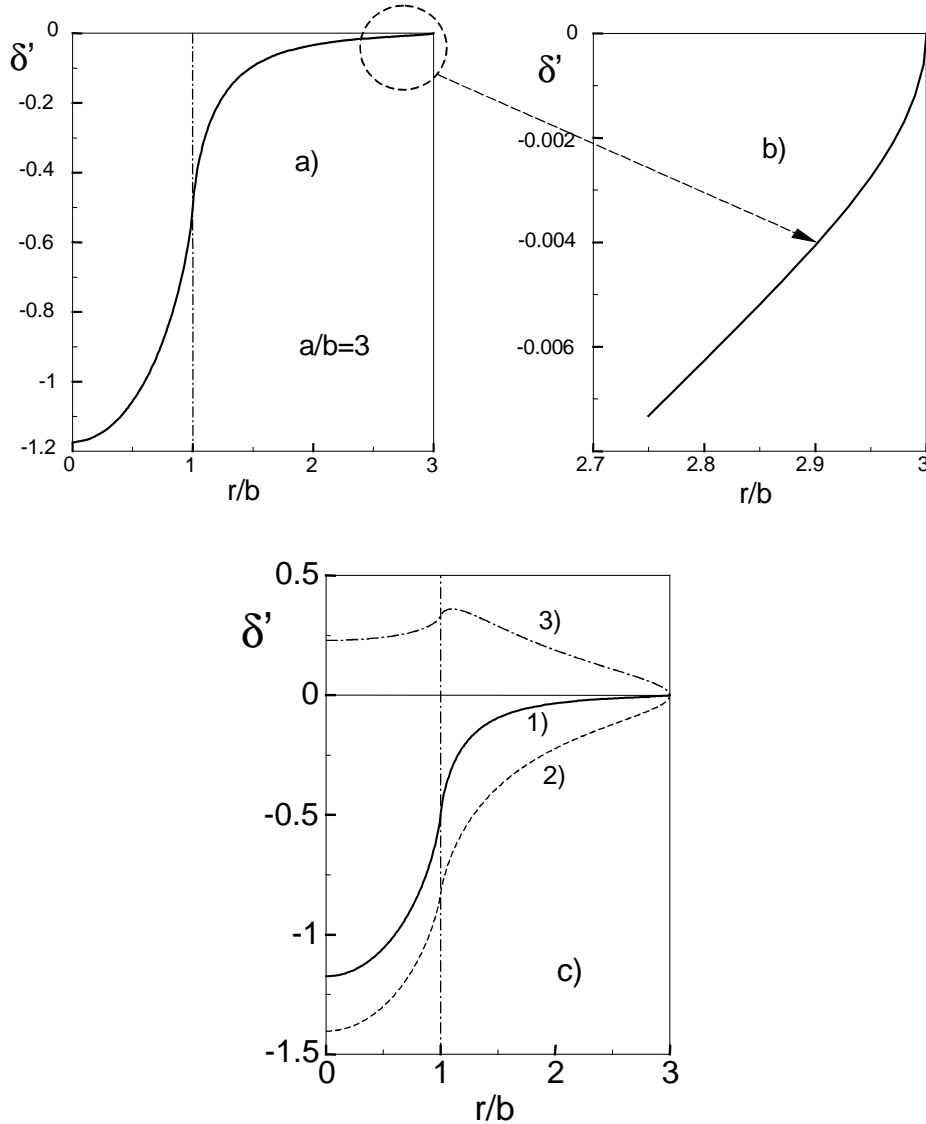

Fig. 3 Residual COD for a crack computed with $f(r/b) = 1$, a), b) crack opening displacements, c) decomposition of displacements: 1) total residual displacement, 2) contribution caused by the stresses in $r < b$, and 3) contribution of the (positive) stress at $r > b$.

Influence of residual stress distribution in r<b

In order to assess the effect of the special shape of the residual stress distribution in the region $r < b$, the residual displacement field was computed for different power-shaped functions $f(r/b) \propto r^n$, resulting in the same stress intensity factor K. Figure 4 shows that the crack opening displacements for the strongly different stress distributions differ hardly. In Fig. 5 the region

near r/b is zoomed. Deviations of 5, 10, and 15% are indicated. Having this in mind, we recommend to use $f(r/b) = 1$ without any loss of accuracy worth mentioning.
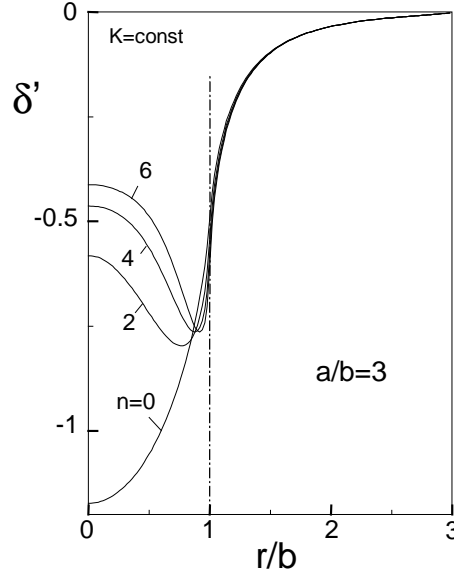

Fig. 4 Crack opening displacement for different residual stress distributions $f(r/b)$ according to eq.(1), yielding the same residual stress intensity factor.
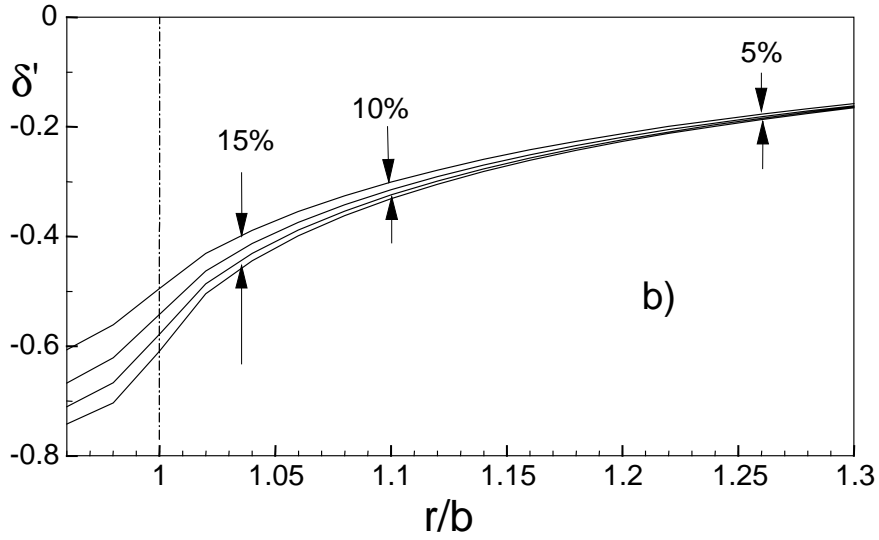

Fig. 5 Deviations of crack opening displacement of Fig. 4 near the location r/b=1.

For $f(r/b) = 1$ the residual displacements δ_1 caused by the stresses at $r/b < 1$ are [5]

$$\delta_1 = -\frac{4ap}{\pi E'}\left[\sqrt{1-\left(\tfrac{r}{a}\right)^2}\,(1-\sqrt{1-\left(\tfrac{b}{a}\right)^2}\,) + \tfrac{b}{a}[\mathbf{E}((\tfrac{r}{b})^2) - E(\arcsin(\tfrac{b}{a},(\tfrac{r}{b})^2)]\right], \quad r < b \qquad (7a)$$

5

$$\delta_1 = -\frac{4ap}{\pi E'}\left[\sqrt{1-(\tfrac{r}{a})^2}\,(1-\sqrt{1-(\tfrac{b}{a})^2}\,) + \tfrac{r}{a}[\mathbf{E}((\tfrac{b}{r})^2) - E(\arcsin\tfrac{r}{a},(\tfrac{b}{r})^2)\right.$$
$$\left. -(1-(\tfrac{b}{r})^2)(\mathbf{K}((\tfrac{b}{r})^2) - F\ \ (\arcsin\tfrac{r}{a},(\tfrac{b}{r})^2))]\right],\quad r>b \tag{7b}$$

and the displacements δ_2 related to the stress distribution in the region $r>b$

$$\delta_2 = \frac{2bp}{\pi E'}\frac{b}{r}\left[E(\arcsin(\tfrac{r}{b}),(\tfrac{b}{r})^2) - E(\arcsin(\tfrac{r}{a}),(\tfrac{b}{r})^2)\right],\quad r<b \tag{8a}$$

$$\delta_2 = \frac{2bp}{\pi E'}\frac{b}{r}\left[\mathbf{E}((\tfrac{b}{r})^2) - E(\arcsin(\tfrac{r}{a}),(\tfrac{b}{r})^2)\right],\quad r>b \tag{8b}$$

with the complete elliptical integrals $\mathbf{E}$ and $\mathbf{K}$ and the incomplete elliptical integrals E and F.

3. Contact stresses

3.1 Contact stress intensity factor and related COD

In a real structure, this is not possible, of course. Prevented crack-face penetration results in a distribution of (positive) contact stresses σ_{cont} which cause a positive contact COD field δ_{cont}

$$\delta_{cont}(r) = \frac{4}{\pi E'} \int_r^a \left(\int_0^{a'} \frac{r'\sigma_{cont}(r')}{\sqrt{a'^2 - r'^2}} \, dr' \right) \frac{da'}{\sqrt{a'^2 - r^2}} \qquad (9)$$

and a contact stress intensity factor

$$K_{cont} = \frac{2}{\sqrt{\pi a}} \int_0^a \frac{r\sigma_{cont}(r)\, dr}{\sqrt{a^2 - r^2}} \qquad (10)$$

This stress intensity factor is positive, since the contact stresses open the crack. The related contact stresses are restricted to a contact area of radius d with $d \cong b$ and must disappear in the region of real (positive) crack opening (see Fig. 6).
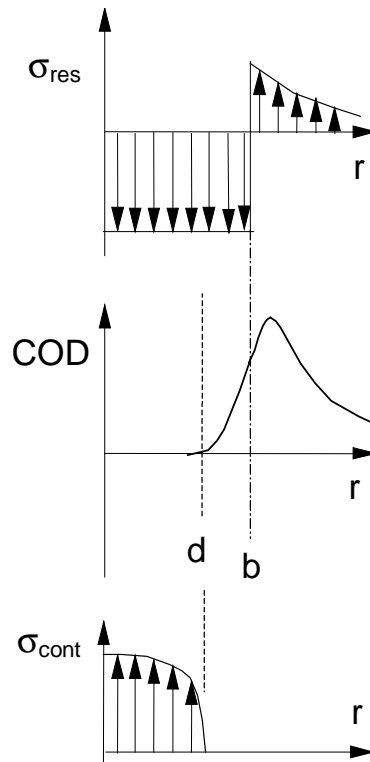

Fig. 6 Contact stresses in the centre region of aVickers crack.

As an example, let us use the residual stress field according to eqs.(1) and (2) with $f(r/b) = 1$. The residual stress intensity factor reads

$$K_{res} = -\frac{2p}{\sqrt{\pi a}}\left(a - \sqrt{a^2 - b^2}\right) + \frac{p}{\sqrt{\pi a}}\left(\frac{b}{a}\right)^2 \sqrt{a^2 - b^2} \qquad (11)$$

The related displacements are shown in Fig. 3a.

3.2 Numerical considerations for the case of $d=b$

For the numerical treatment, a power series expansion (truncated after the term N) of the unknown contact stresses is applied according to

$$\sigma_{cont} = \begin{cases} \displaystyle\sum_{n=0}^{N} A_n r'^n & for \quad r' \le d \\ 0 & else \end{cases} \qquad (12)$$

Introduction in (9) yields

$$\delta_{cont} = \frac{4}{\pi E'} A_n \int_r^a I_n(a') \frac{da'}{\sqrt{a'^2 - r^2}} = \frac{4}{\pi E'} A_n J_n \qquad (13)$$

with the analytically given inner integrals (see 236.2 in [6])

$$I_n = \int_0^{min(a',d)} \frac{r'^{n+1}}{\sqrt{a'^2 - r'^2}} dr' \qquad (14)$$

In order to make the procedure transparent, it is restricted to the first three terms in the series representation (12) only. The first inner integrals read

$$I_0 = \begin{cases} a' & for \quad a' \le d \\ a' - \sqrt{a'^2 - d^2} & for \quad a' > d \end{cases} \qquad (15)$$

$$I_1 = \begin{cases} \frac{1}{4} a'^2 \, \pi & for \quad a' \le d \\ -\frac{1}{2} d \sqrt{a'^2 - d^2} + \frac{1}{2} a'^2 \arcsin\frac{d}{a'} & for \quad a' > d \end{cases} \qquad (16)$$

$$I_2 = \begin{cases} \frac{2}{3} a'^3 & for \quad a' \le d \\ \frac{2}{3} a'^3 - a'^2 \sqrt{a'^2 - d^2} + \frac{1}{3}(a'^2 - d^2)^{3/2} & for \quad a' > d \end{cases} \qquad (17)$$

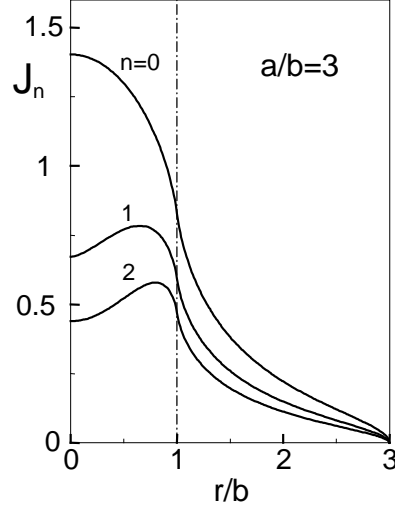The first integrals J_n ($n=1$-3) defined by eq.(13) are shown in Fig. 7 for a crack of $a/b=3$.

Fig. 7 First integrals defined by eq. (13).

The unknown coefficients A_n can determined exclusively from the condition $\delta_{total} = 0$ for $r < d$. The integral J_n and the residual displacements were evaluated at $m > N$ equidistant points in $0 < r < b$. A least squares procedure was applied, which minimised the expression

$$\left(\delta_{res}(r) + \sum_{n=0}^{N} A_n(a/b) J_n(a/b, r/b)\right)^2 = \min \tag{18}$$

providing A_n. Figure 8a shows the increasing approximation of the residual displacements by the (plotted in negative direction) contact displacements computed with an increasing number of terms in eq.(12). After 5 terms already are the deviations hardly visible. In Fig. 8b the related contact stresses are plotted for $d=b$ as a function of the number of used terms. The computations were performed for different values of $d \approx b$. It was found that for the computation of the contact displacement field at $r > \max(d,b)$ no significant influence of d was detectable. Therefore, we restricted our considerations to $d=b$.

From a convergence study as illustrated in Fig. 8, it was found that the contact stress for our example can be adequately expressed by

$$\sigma_{cont} = D(1 - (r/b)^q) \tag{19a}$$

(see Fig. 8c). By introducing this type of stress distribution in eq.(9) and minimising $(\delta_{res} + \delta_{cont})^2$, an improved solution was found as plotted in Fig. 9 for several values of q. The parameters D and q resulting for several ratios a/b are given in Fig. 10 and approximated by

$$D \cong 0.898 + 0.1127\,b/a \tag{19b}$$

$$q \cong 5.32 + 2.69\,b/a + 13.33\,(b/a)^2 \tag{19c}$$

The contact displacements were computed using the approximate contact stress solution eq.(19). The resulting δ_{cont} are shown in Fig. 11 together with the residual displacements δ_{res}.
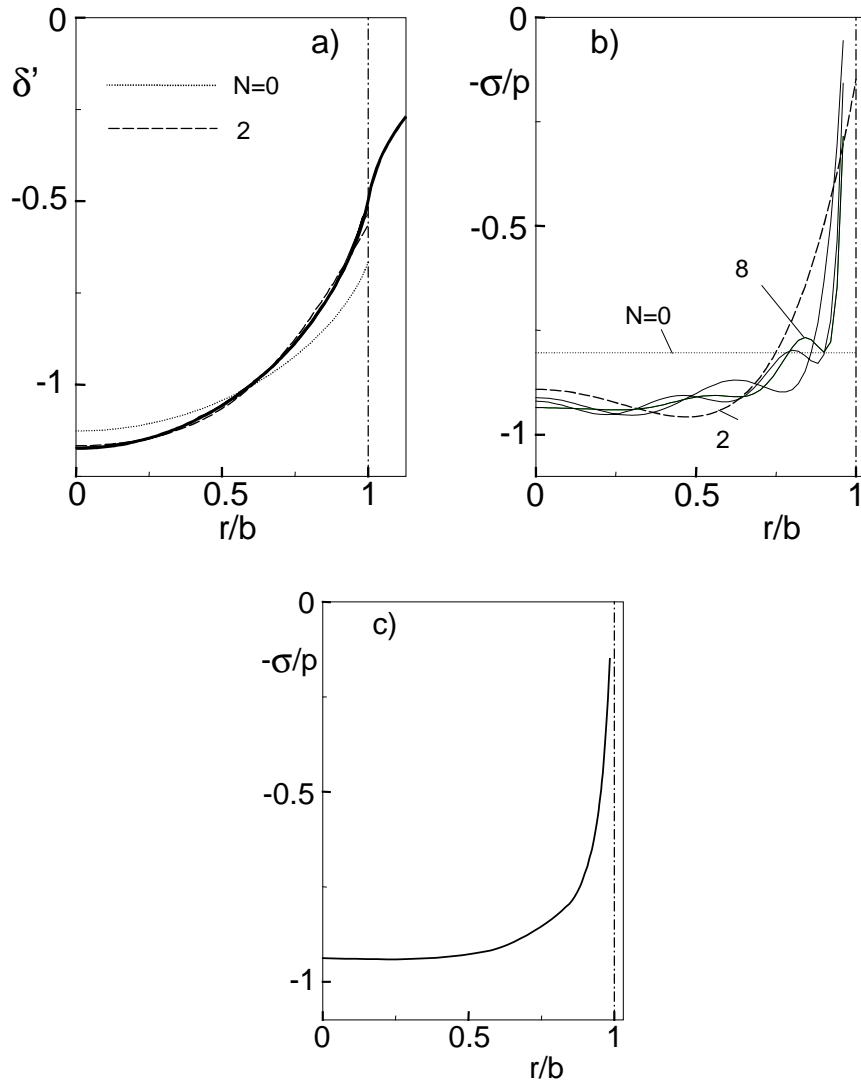
9

Fig. 8 a) Approximation of the total displacements by an increasing number of terms in eq.(13), b) contact stresses for *N*=0-8, c) asymptotic solution, (*a*/*b*=3).
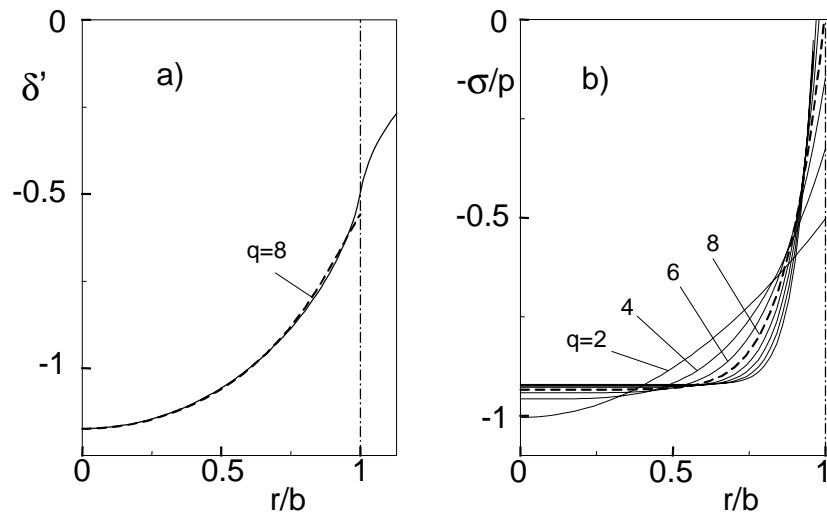

Fig. 9 a) Approximation of the residual displacements by stresses of the type of eq.(19), b) representation of the stresses.
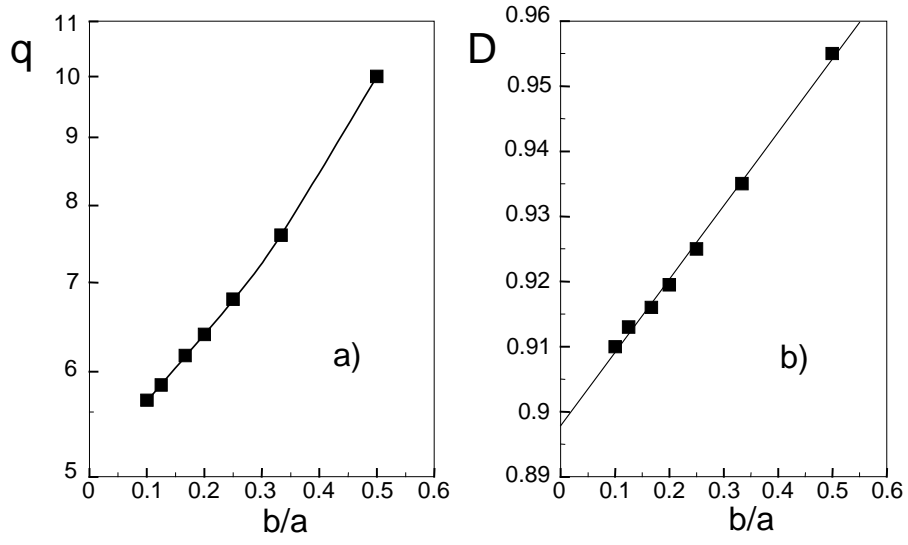
Fig. 10 Parameters for the contact stress distribution, eq.(19).

4. Total stress intensity factor and total COD

4.1 Results for *d=b*

The really active total stress intensity factor is then

$$K_{total} = K_{res} + K_{cont} \tag{20}$$

and the total crack opening displacements are given by

$$\delta_{total}(r) = \frac{4}{\pi E'} \int_r^a \left(\int_0^{a'} \frac{r'\sigma_{total}(r')}{\sqrt{a'^2 - r'^2}} dr' \right) \frac{da'}{\sqrt{a'^2 - r^2}} \tag{21}$$

with

$$\sigma_{total} = \sigma_{res} + \sigma_{cont} \tag{22}$$

The total displacements δ_{total} were found by superposition of these two solutions (Figs. 11b, 11c).
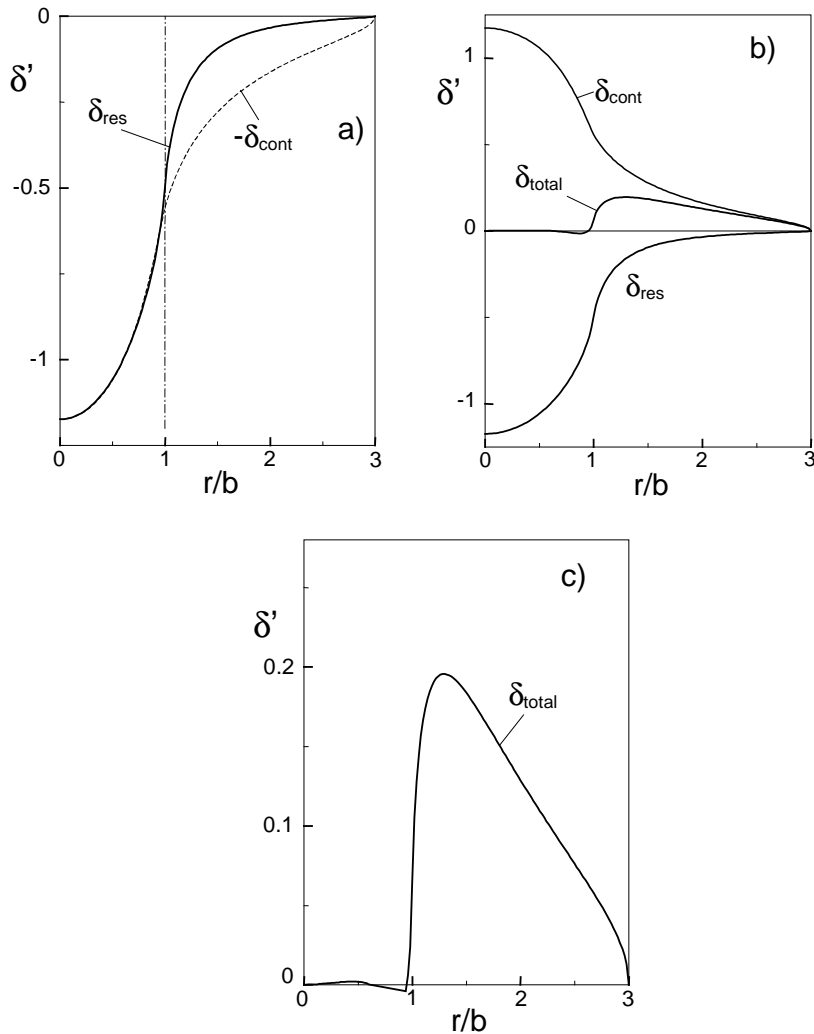

Fig. 11 a) Fitting of the displacements in $0<r<b$, b) and c) total displacements δ_{total} obtained by superposition of the residual and contact displacements.

The small deviations from $\delta_{total} = 0$ in $0 \leq r \leq b$ indicate the slight differences between the correct and the approximate contact stress solutions (i.e. the differences visible in Fig. 9a).

Total displacements are represented in Fig. 12a for several relative crack lengths a/b. This figure is recommended for interpolation in $2.5 \leq a/b \leq 5$. The related (normalised) total stress intensity factor is plotted in Fig. 12b, exhibiting the well-established proportionality $K \propto a^{-3/2}$ for $a/b \geq 2.5$

$$K' \cong \frac{0.372}{(a/b)^{3/2}} \qquad (23)$$

Relation (23) allows to estimate the pressure p from the experimentally determined dependency between indentation load P and crack size
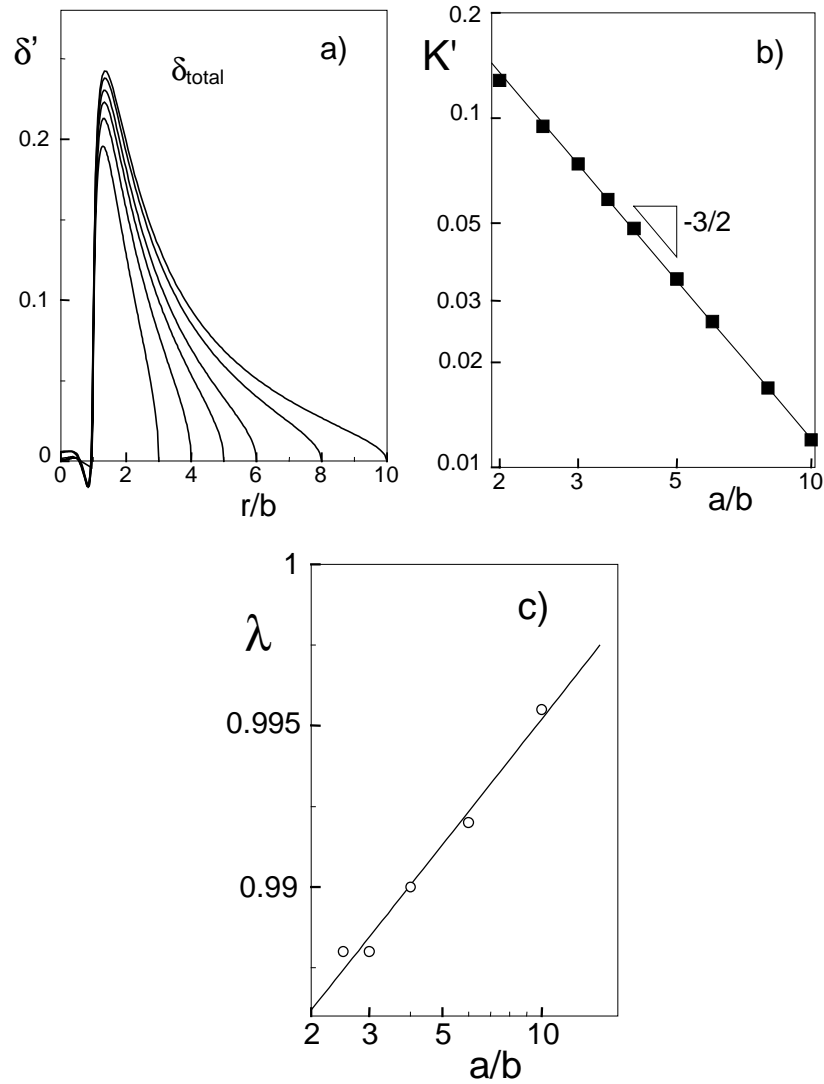
$$K = \chi \frac{P}{a^{3/2}} \qquad (24)$$

Fig. 12 a) Total crack opening displacement, b) normalised total stress intensity factor c) coefficient λ for eq.(25).

13

4.2 Influence of the contact zone radius *b*

For the preceding computation, it was made use of the fact that the contact zone is close to the region of compressive residual stresses, i.e. *d≅b*. For these computations, it was assumed *d=b*. In order to illustrate the influence of the value *d*, the computations were repeated for *d=0.95b* and *d=1.05b*. The resulting displacements δ' are plotted in Fig. 13a for *a/b=3*. A slight influence of *d* can be seen. The same effect was obtained for the normalised stress intensity factor *K'*. In Fig. 13b the ratio δ'/*K'* is represented. No difference is visible in the region *r>b*.
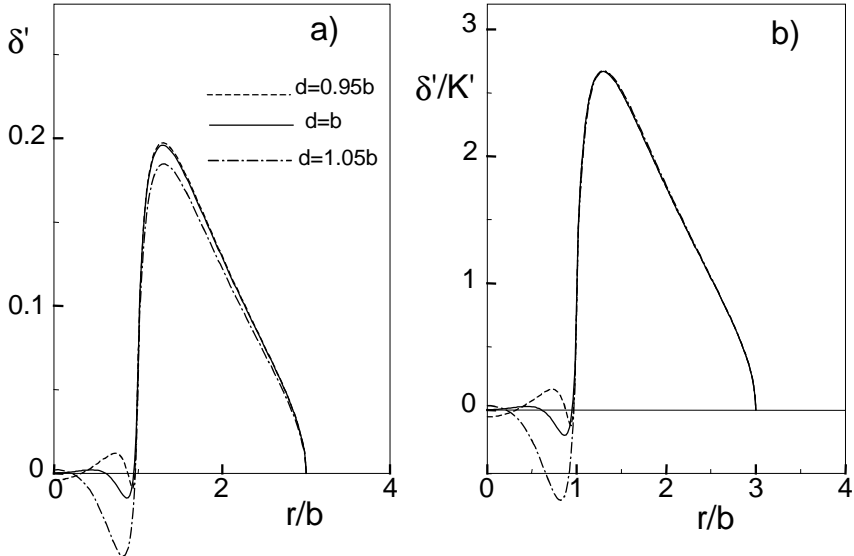

Fig. 13 Influence of the contact zone radius.

5. Approximated COD field

Based on the preceding considerations, an approximate analytical description of the total crack opening displacement can be given by

$$\delta_{total} \cong -\frac{4ap}{\pi E'} g_1(a,b,r) + \frac{2bp}{\pi E'} g_2(a,b,r) + \frac{4ap*}{\pi E'} g_1(a,\lambda b,r) \tag{25}$$

with

$$g_1(a,b,r) = \sqrt{1-(\tfrac{r}{a})^2}(1-\sqrt{1-(\tfrac{b}{a})^2}) + $$
$$+ \tfrac{r}{a}[\mathbf{E}((\tfrac{b}{r})^2) - E(\arcsin\tfrac{r}{a},(\tfrac{b}{r})^2) - (1-(\tfrac{b}{r})^2)(\mathbf{K}((\tfrac{b}{r})^2) - F(\arcsin\tfrac{r}{a},(\tfrac{b}{r})^2))] \tag{26a}$$

$$g_2(a,b,r) = \tfrac{b}{r}[\mathbf{E}((\tfrac{b}{r})^2) - E(\arcsin(\tfrac{r}{a},(\tfrac{b}{r})^2)] \tag{26b}$$

$$p*/p \cong 0.635 + 0.319 b/a \tag{27}$$

$$\lambda \cong 0.9828 (a/b)^{0.00565} \tag{28}$$

with λ represented in Fig. 12c. The unknown quantity p may be determined from the total stress intensity factor

$$K_{total} \cong \frac{2(p*-p)}{\sqrt{\pi a}}\left(a - \sqrt{a^2-b^2}\right) + \frac{p}{\sqrt{\pi a}}\left(\frac{b}{a}\right)^2 \sqrt{a^2-b^2} \tag{29}$$

in combination with Fig. 12b or eq.(23).

Having in mind the slight influence of the stress distribution in the contact zone on the displacements (see e.g. Fig. 5) we restrict the solution (25) to $r > 1.25b$ and $2.3 < a/b < 10$.

Expressed by the stress intensity factor, the displacements read

$$\delta = \frac{4K\sqrt{a}}{0.382\,\pi E'}\left(\frac{a}{b}\right)^2\left[\frac{b}{2a} g_2(a,b,r) + (0.635 + 0.319 b/a)g_1(a,b,r) - g_1(a,\lambda b,r)\right] \tag{30}$$

A representation of the crack opening displacement in the normalised form δ'/K' is given in Fig. 14. This plot is appropriate for performing interpolations with respect to r/b and a/b. The data of Table 1 allow interpolations using bi-cubic splines.

A FORTRAN program for the computation of the normalised COD δ'/K' is given in the Appendix.
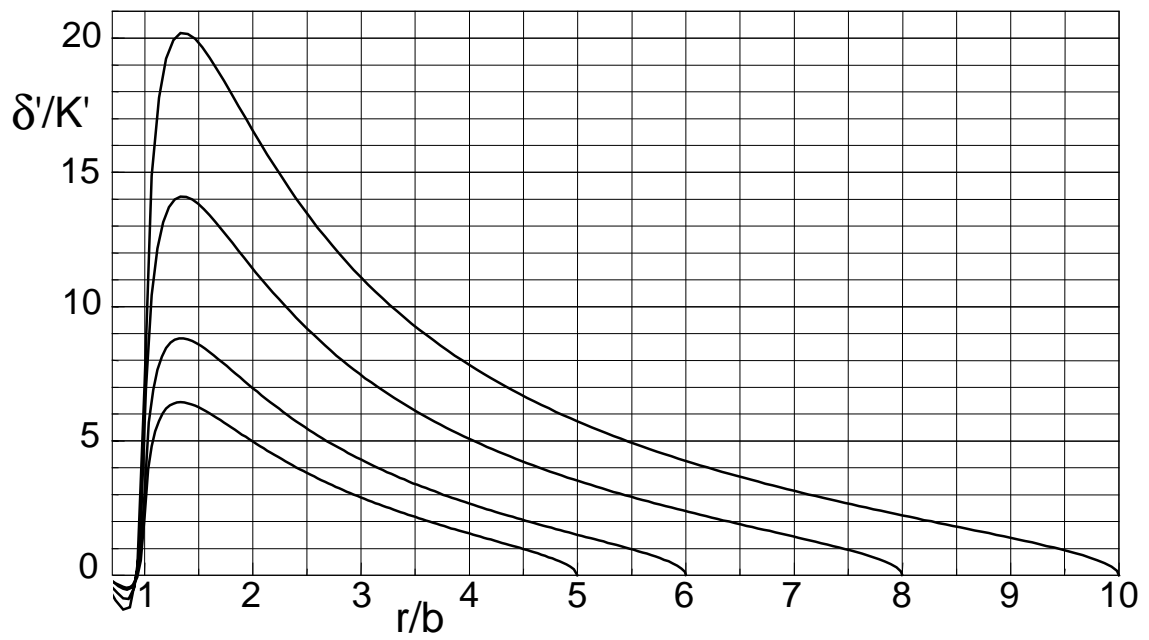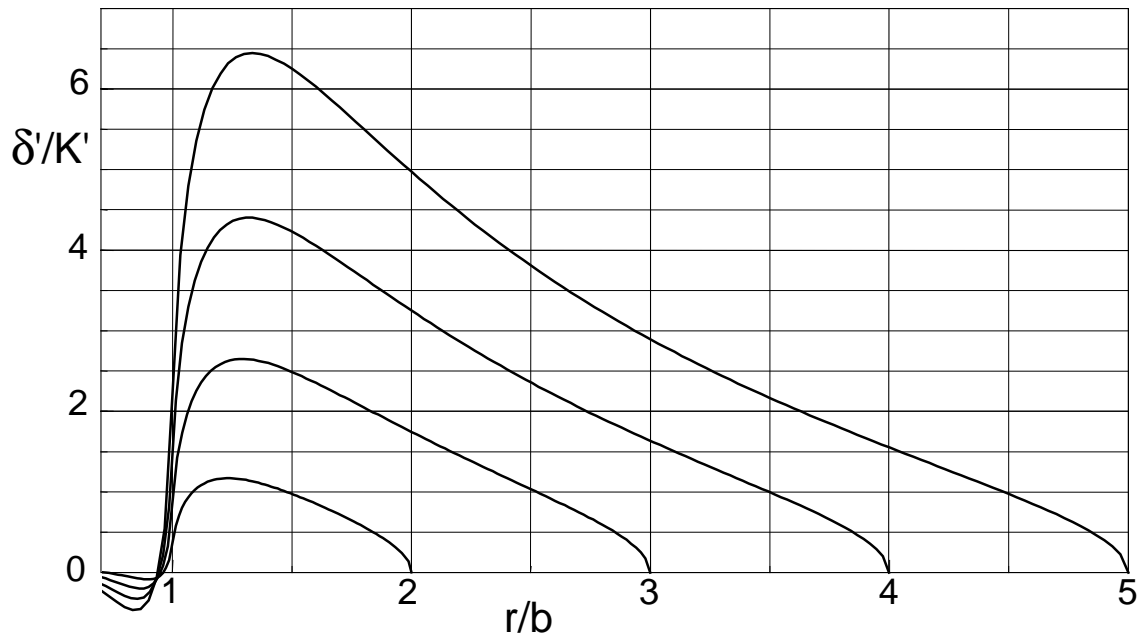
Fig. 14 Normalised COD appropriate for interpolations.

16

6. Near-tip displacements

In practical applications, for instance, the determination of the "crack-tip toughness" K_{I0}, it is of interest to know the near-tip displacement field. A simple relation for the COD can be derived by replacing the inner integrals in (5), (9), and (21) by the stress intensity factors $K(a')$

$$\delta_{total}(r) = \frac{2}{\sqrt{\pi E'}} \int_r^a \frac{K_{total}(a')\sqrt{a'}\,da'}{\sqrt{a'^2 - r^2}} \tag{31}$$

Application of the mean value theorem for integrals then yields

$$\delta_{total}(r) = \frac{2\sqrt{\alpha}}{\sqrt{\pi E'}} K(\alpha) \int_r^a \frac{da'}{\sqrt{a'^2 - r^2}} = \frac{2\sqrt{\alpha}}{\sqrt{\pi E'}} K(\alpha) \ln \frac{a + \sqrt{a^2 - r^2}}{r} \tag{32}$$

with a certain intermediate crack length $r \leq \alpha \leq a$. For $r \to a$ we can replace α by a and obtain for the near-tip displacements

$$\delta_{tip}(r) = \frac{2\sqrt{a}}{\sqrt{\pi E'}} K(a) \ln \frac{a + \sqrt{a^2 - r^2}}{r} \tag{33}$$

A series expansion of eq.(25) gives

$$\frac{\delta'}{K'} = A\sqrt{x} + Bx^{3/2} + Cx^{5/2}, \quad x = 1 - r/a \tag{34}$$

with the coefficients

$$A = \sqrt{\pi/2}\,\sqrt{a/b} \tag{35}$$

$$B \cong 0.011 + 1.8197\ln(a/b) \tag{36}$$

$$C \cong -0.6513 + 2.121\ln(a/b) \tag{37}$$

with $2.5 < a/b < 10$ for B and C.

By exclusive use of the first coefficient A, the well-known Irwin relation results

$$\delta_{tip} = \sqrt{\frac{8}{\pi}} \frac{K_{tip}}{E'} \sqrt{a - r} \tag{38}$$

A comparison of the crack-tip approximations, eqs.(34-37), with the numerical results is made in Figs. 15a and 15b. In Fig. 15c, the numerical solution, approximation (33) and the Irwin relation (38) are compared. The best solution, of course, is the one given by eqs.(34-37). Irrespective of the actual a/b ratio, the best solution is eq.(33).
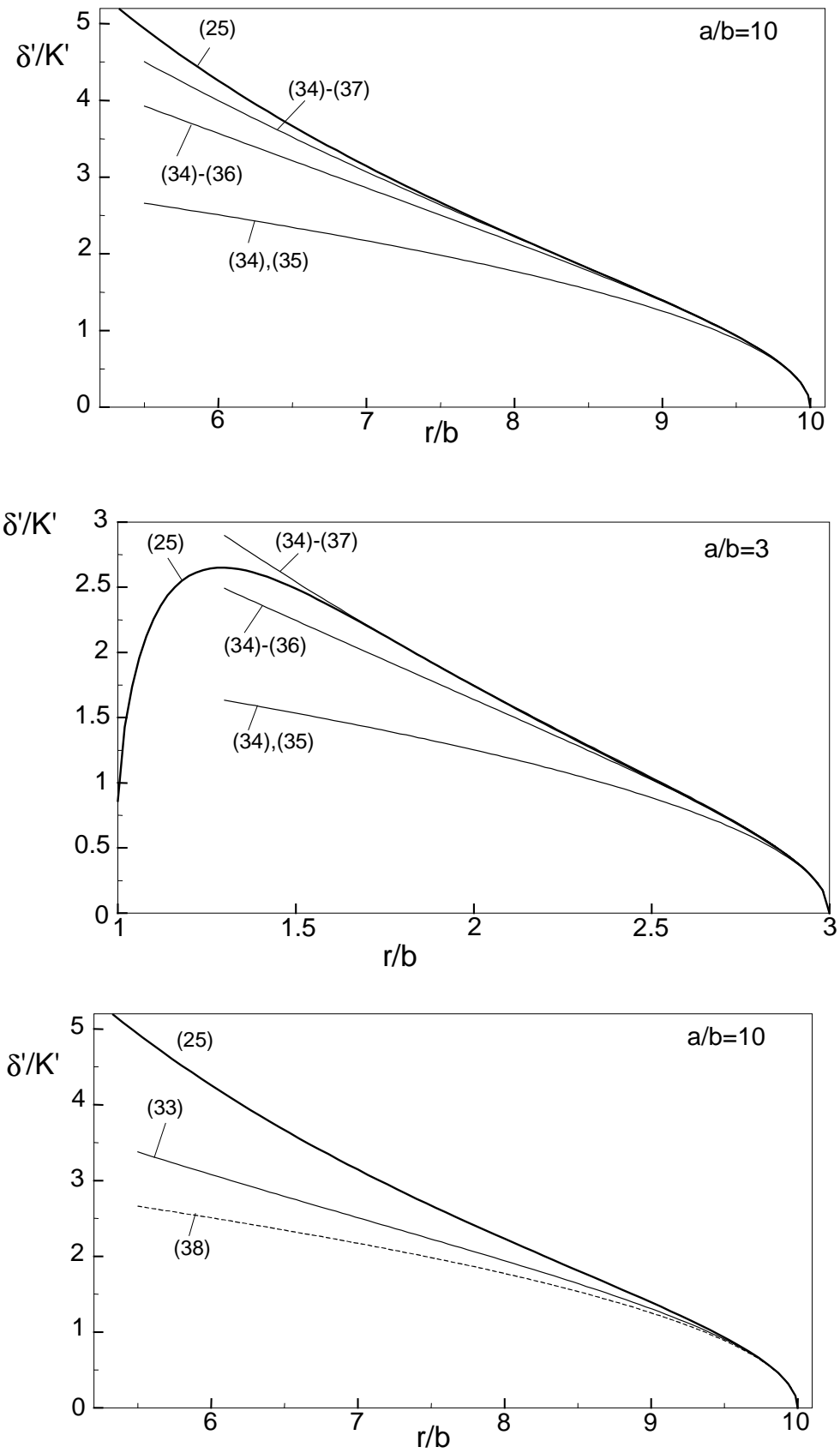
Fig. 15 Comparison of the normalised COD with different crack-tip approximations.

r/b	a/b=3	4	5	6	8	10
1.2	2.586	4.254	6.196	8.45	13.48	19.23
1.4	2.599	4.360	6.410	8.78	14.07	20.16
1.6	2.353	4.056	6.029	8.31	13.41	19.28
2	1.745	3.252	4.976	6.96	11.42	16.55
2.5	1.032	2.355	3.809	5.46	9.26	13.47
3	0	1.635	2.896	4.30	7.49	11.09
3.5		1.00	2.167	3.39	6.11	9.26
4		0	1.551	2.67	5.07	7.83
5			0	1.50	3.51	5.73
6				0	2.38	4.26
8					0	2.23
10						0

Table 1 Normalised displacements δ'/K' for interpolation with bi-cubic splines.

References

[1] Munz, D, Fett, T., CERAMICS, Failure, Material Selection, Design, Springer-Verlag, Heidelberg, 1999.

[2] Rödel, J., Rissüberbrückung in keramischen Werkstoffen, VDI-Verlag, Reihe 5: Grund- und Werkstoffe, Nr. 331, Düsseldorf 1993.

[3] Hill, R., Mathematical Theory of Plasticity, Oxford University Press, 1950, Oxford

[4] Evans, A.G., Charles, E.A., Fracture toughness determinations by indentation, J. Am. Ceram. Soc. **59**(1976), 371–372.

[5] Gröbner, W, Hofreiter, N., Integraltafeln I, Springer Verlag, 1975, Heidelberg.

[6] Fett, T., Munz, D., Stress intensity factors and weight functions, Computational Mechanics Publications, 1997, Southampton.

[7] Timoshenko, S.P., Goodier, J.N., Theory of Elasticity, 1970, McGraw-Hill, Kogakusha.

[8] Harwell Subroutine Library, A Catalogue of Subroutines, Computer Science and Systems Division, AERA, Harwell 1981.

Appendix

A1. Crack opening under pure displacement boundary conditions

The residual stress problem considered before was treated under pure stress boundary conditions. For the computation of the crack opening displacements by eq.(5), we applied the weight function technique with a weight function h

$$h \propto \frac{1}{\sqrt{a^2 - r^2}} \qquad (A1)$$

where now integration has to be performed over the crack area instead of the crack length, i.e. $\propto r\mathrm{d}r$ instead of r. This is a typical weight function for stress boundary problems in which the stresses are not affected by the crack opening. In the present case, the compressive residual stresses will decrease with increasing COD, because the extension of the stress field is limited. A correct analysis would be possible by using a weight function for mixed boundary conditions. Unfortunately, such a weight function is not available. Nevertheless, it is possible to consider the two limit cases:

- Crack opening under pure stress conditions using the stresses which are present in the uncracked body only (Fig. A1a). This problem was dealt within the preceding chapters for $\sigma_{res} = const.$ in $0 < r < b$.

- Crack opening under pure displacement conditions $\delta_{res} = const.$ in $0 < r < b$ (Fig. A1b).
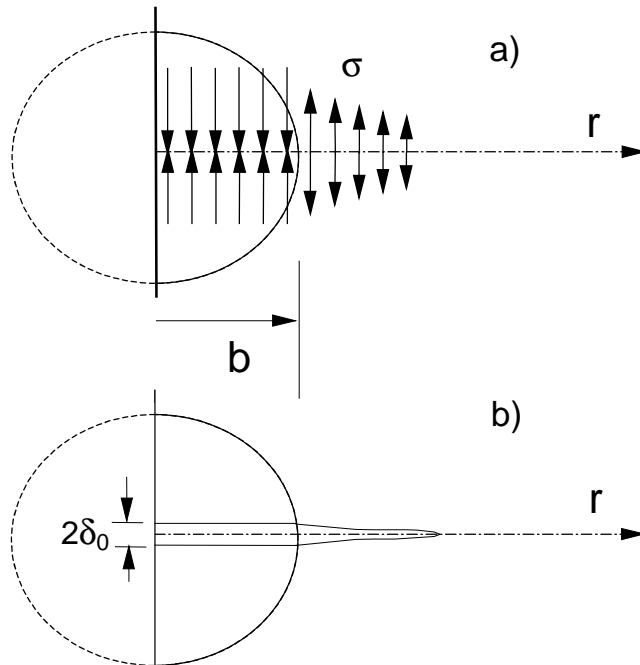

Fig. A1 a) Limit case of pure stress boundary conditions, b) limit case of pure displacement conditions.

In order to compute the displacements outside of the plastic zone (i.e. for $r > b$), the stresses have to be computed, which produce the displacement $\delta = \delta_0$ in $0 < r < b$. The stress distribution

which causes constant displacements δ_0, can be approximated sufficiently by the displacements of a rigid stamp pressed into a plane surface, i.e. the crack surface (see e.g. [7])

$$p(r) \cong p_0 \frac{b}{\sqrt{b^2 - r^2}} \tag{A2}$$

exhibiting a stress singularity for $r \to b$ as shown in Fig. A2 as the dashed curve. Introducing these stresses into eq.(5) yields for $r > b$

$$\delta \cong \frac{4ap_0}{\pi E'} \int_r^a \frac{\text{Artanh}(b/a')}{\sqrt{a'^2 - r^2}} da' \tag{A3}$$
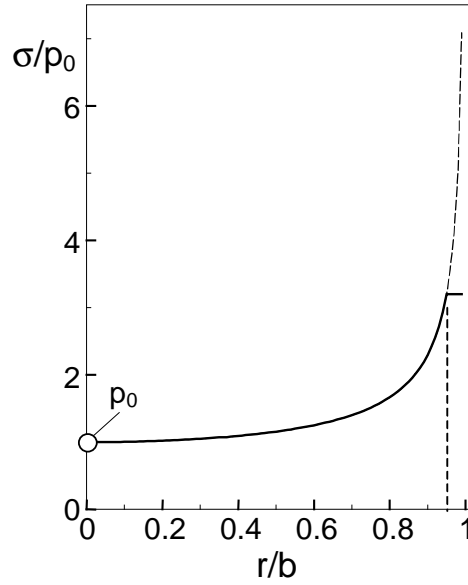
Fig. A2 Stress distribution producing constant displacements in $0 < r < b$.

The displacements are represented in Fig. A3a. Figure A3b shows the displacements δ', now defined as

$$\delta' = \frac{\pi E'}{4ap_0} \tag{A4}$$

normalized to the stress intensity factor K' defined by

$$K' = \frac{K}{p_0 \sqrt{b}} \tag{A5}$$

In Fig. A4, the displacements according to eq.(A3) are compared with those caused by pure stress conditions. It can be concluded that the two solutions differ by less than 5% for $(r-b)/(a-b) > 0.5$.

In the case of displacement boundary conditions, the effective visible COD shows a sharp maximum near $r/b \approx 1$.

In order to estimate the influence of the mixed boundary conditions, the two solutions for pure stress and pure displacement are superimposed

$$\delta = \beta\delta_\sigma + (1-\beta)\delta_\delta \quad , \quad 0 \le \beta \le 1 \tag{A6}$$

where δ_σ stands for the solution under stress conditions and δ_δ for the solution under pure displacement conditions. The displacements computed with eq.(A6) are plotted in Fig. A5.
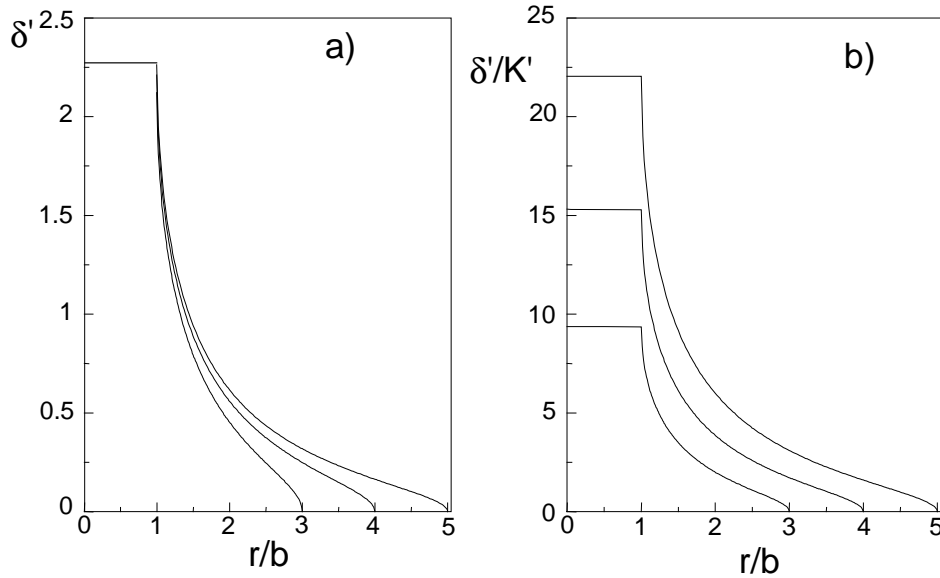
Fig. A3 a) Crack opening profile $\delta'(r)$ for a half-penny-shaped crack opened under a constant displacement in the zone $0<r<b$, b) displacements δ' normalized to the stress intensity factor K'.
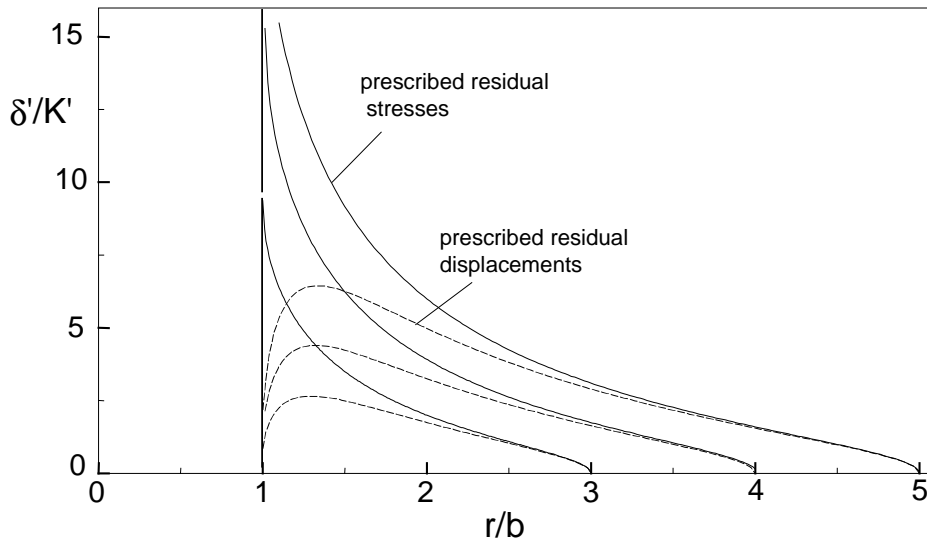
Fig. A4 Curves from Fig. 14 compared with results from Fig. A3b.

22

Fig. A5 Interpolation of the limit cases of stress and displacement boundary conditions according to eq.(A6) for stresses given by eq.(A2).

A2. Displacement boundary conditions with non-singular stresses

As can be seen from eq.(A2), the stresses become infinite for $r \rightarrow b$. This is, of course, not possible in real materials. Stresses are reduced, for instance, by exceeding the yield stress. To illustrate the influence of a disappearing stress singularity, let us consider the modified stress distribution which is cut at $r = \kappa b$

$$\sigma = \begin{cases} p_0 \dfrac{b}{\sqrt{b^2 - r^2}} & for \quad r \leq \kappa b \\[4mm] p_0 \dfrac{1}{\sqrt{1 - \kappa^2}} & for \quad r > \kappa b \end{cases} \tag{A7}$$

This distribution is entered in Fig. A2 as the solid curve. Introducing these stresses into eq.(5) yields the normalized displacements δ' as shown in Fig. A6a and the ratio δ'/K' as shown in Fig. A6b for $\alpha = 0.95$. The influence of the parameter κ can be seen from Fig. 6c and Fig. 6d. The interpolation of the limit cases according to eq.(A6) results in the displacement curves shown in Fig. A7. As has to be expected, only the displacements near $r = b$ are influenced by the modified stress distribution.

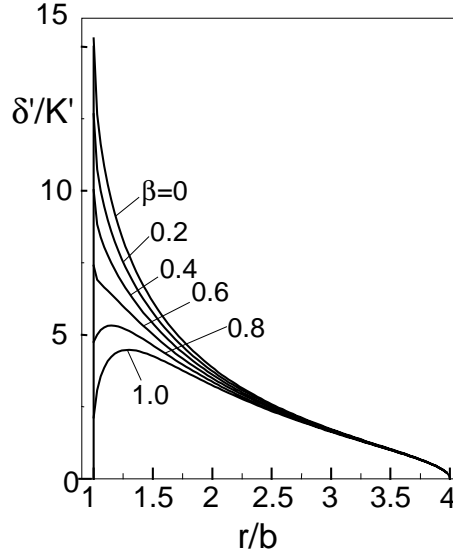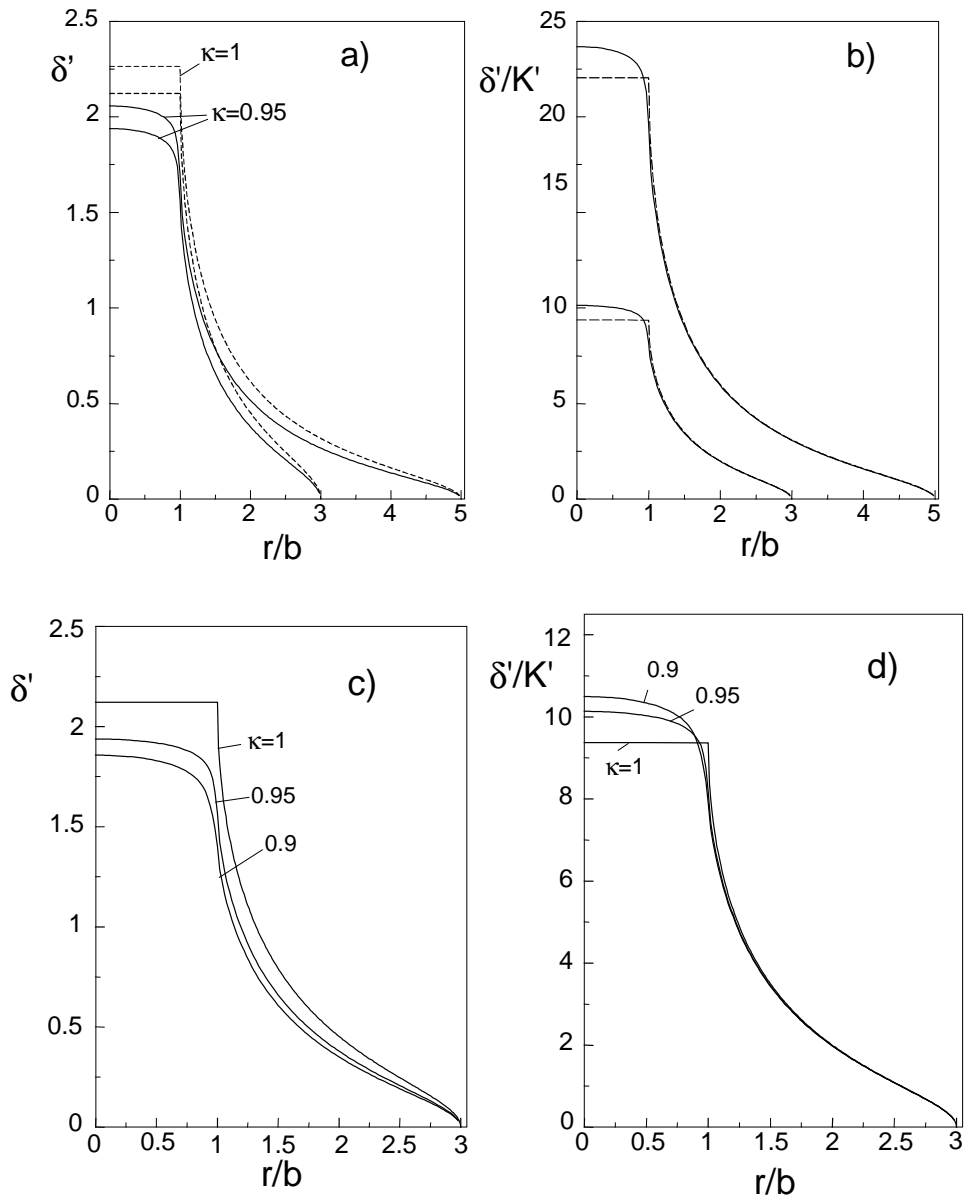**Fig. A6** Displacements computed with the non-singular stress distribution eq.(A7).
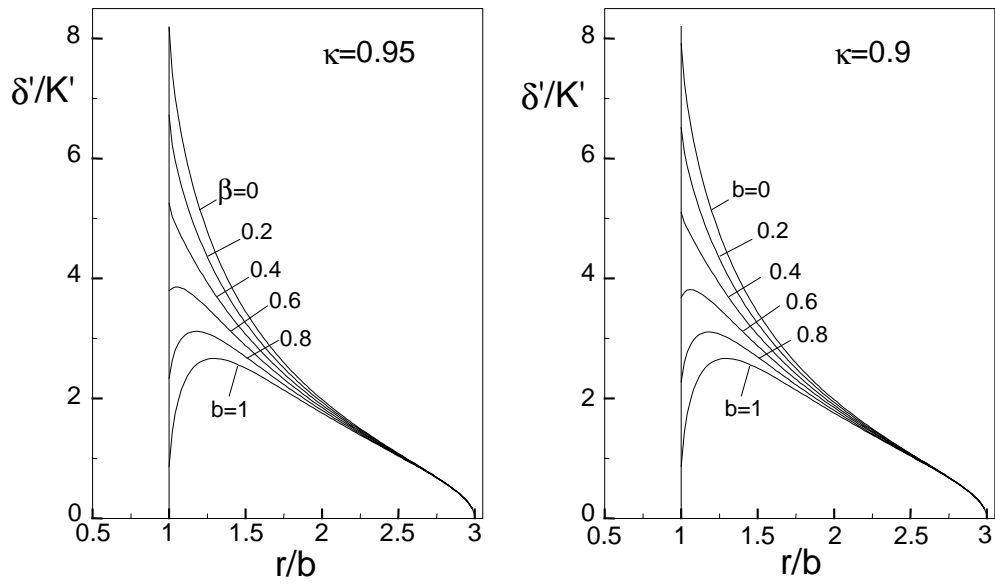
Fig. A7 Interpolation of the limit cases of stress and displacement boundary conditions according to eq.(A6) for stresses given by eq.(A7).

A3. Computation of the crack profile

The following program computes the relative COD given as "drel"=δ'/K'. In the program, the contact zone radius b is set to $b=1$. The crack size a is chosen to be variable, i.e. a is identical with the ratio a/b.

The subroutines FB02AD and FB01AD are routines of the HARWELL program library [8].

```
      IMPLICIT REAL*8 (A-H,O-Z)
      open (9,file='p02.dat',status='old',access='append')
      PI=4.d0*datan(1.d0)
      b=1.d0
      a=3.d0
      am1=a-1.d0
      do 50 i=1,200
      r=1.d0+am1/200.d0*(i-1)
      CALL displ(a,b,r,delta,ak)
      drel=delta/ak
      write(6,101) r,delta,drel
      write(9,101) r
      write(9,101) drel
c     write(9,101) dr1
   50 CONTINUE
101 FORMAT(1H 5F14.6)
      STOP
      END

C     ************************************************************

      SUBROUTINE displ(a,b,r,delta,aks)
      IMPLICIT REAL*8 (A-H,O-Z)
      PI=4.D0*DATAN(1.D0)
      CALL FUNKT(a,b,r,ds1,ds2)
      alam=0.9828d0*(a/b)**0.00565d0
      b1=alam*b
      CALL FUNKT(a,b1,r,ds3,ds0)
      res1=-a*ds1
      res2=0.5d0*b*ds2
      res=res1+res2
      pstern=0.635d0+0.319d0/a
      dcont=ds3*a*pstern
      delta=dcont+res
      ak=2.d0*(pstern-1.d0)/dsqrt(pi*a)*(a-dsqrt(a**2-b**2))+
     . 1.d0/dsqrt(pi*a)*(b/a)**2*dsqrt(a**2-b**2)
      aks=ak/dsqrt(b)
      RETURN
      END

C     ************************************************************

      SUBROUTINE FUNKT(a,b,r,ds1,ds2)
      IMPLICIT REAL*8 (A-H,O-Z)
      PI=4.D0*DATAN(1.D0)
      opt=3.d0
      bdr=b/r
      rda=r/a
      bda=b/a
      emsq=bdr**2
      cosp=dsqrt(1.d0-rda**2)
      call fb02ad(emsq,rda,cosp,EE,FF)
      call fb01ad(emsq,opt,vk,ve)
```

```
      ds1=dsqrt(1.d0-rda**2)*(1.d0-dsqrt(1.d0-bda**2))+rda*(ve-ee
     . -(1.D0-BDR**2)*(vk-ff))
      ds2=(ve-ee)/r
      RETURN
      END



C     ************************************************************


      SUBROUTINE FB01AD(C,B,VK,VE)
C STANDARD FORTRAN 66 (A VERIFIED PFORT SUBROUTINE)
      DOUBLE PRECISION B,C,D,E,VE,VK,XLG
      DATA XLG/.723700557733226211D+76/
      D=1.0D0-C
      IF(D .GT. 0.0D0)E=-DLOG(D)
      IF(B .LT. 2.0D0)GO TO 1
      IF(C .GE. 1.0D0)GO TO 2
          VE=E*(((((((((((
     A    3.18591956555015718D-5*D  +.989833284622538479D-3)*D
     B    +.643214658643830177D-2)*D +.16804023346363385D-1)*D
     C    +.261450147003138789D-1)*D +.334789436657616262D-1)*D
     D    +.427178905473830956D-1)*D +.585936612555314917D-1)*D
     E    +.937499997212031407D-1)*D +.249999999999901772D0)*D)
     F    +((((((((((
     G    .149466217571813268D-3*D  +.246850333046072273D-2)*D
     H    +.863844217360407443D-2)*D+.107706350398664555D-1)*D
     I    +.782040406095955417D-2)*D +.759509342255943228D-2)*D
     J    +.115695957452954022D-1)*D +.218318116761304816D-1)*D
     K    +.568051945675591566D-1)*D +.443147180560889526D0)*D
     L    +1.0D0
       GO TO 1
    2 VE=1.0D0
    1 IF(B .EQ. 2.0D0)GO TO 3
      IF(C .GE. 1.0D0)GO TO 4
          VK=E*((((((((((((
     A    .297002809665556121D-4*D  +.921554634963249846D-3)*D
     B    +.597390429915542916D-2)*D +.155309416319772039D-1)*D
     C    +.239319133231107901D-1)*D +.301248490128989303D-1)*D
     D    +.373777397586236041D-1)*D +.488280419068623980D-1)*D
     E    +.703124997390383521D-1)*D +.124999999999908081D0)*D
     F    +.5D0)+((((((((((
     G    .139308785700664673D-3*D  +.229663489839695869D-2)*D
     H    +.800300398064998537D-2)*D +.984892932217689377D-2)*D
     I    +.684790928262450512D-2)*D +.617962744605331761D-2)*D
     J    +.878980187455506468D-2)*D +.149380135326871652D-1)*D
     K    +.308851462713051899D-1)*D +.965735902808562554D-1)*D
     L    +1.38629436111989062D0
       GO TO 3
    4 VK=XLG
    3 RETURN
      END



C     ************************************************************


      SUBROUTINE FB02AD(CAYSQ,SINP,COSP,E,F)
C STANDARD FORTRAN 66 (A VERIFIED PFORT SUBROUTINE)
      DOUBLE PRECISION A,CAYDSQ,CAYMOD,CAYSQ,CFI,CFI1,
     1CFJ,CFJ1,CFL,CFM,CFN,COSP,CRIT,DEL1,DEL2,DEL3,DEL4,
```

27

```
  2E,F,FACT,FACTM,FACTN,FACTOR,FACTRO,FACT1,FLOG1,H,
  3H1,PHI,RECIP,SIG1,SIG2,SIG3,SIG4,SINP,SIN2,TERM,T1,T2
    PHI=DATAN(SINP/COSP)
    IF(CAYSQ*SINP*SINP-0.5D0)1,1,5
  1 H=1.0D0
    A=PHI
    N=0
    SIG1=0.D0
    SIG2=0.D0
    SIN2=SINP*SINP
    TERM=SINP*COSP*0.5D0
    CRIT=PHI
  2 N=N+1
    RECIP=1.0D0/FLOAT(N)
    FACT=(FLOAT(N)-.5D0)*RECIP
    H1=H
    H=FACT*CAYSQ*H
    A=FACT*A-TERM*RECIP
    TERM=TERM*SIN2
    CRIT=CRIT*SIN2
    DEL1=H*A
    DEL2=-.5D0*RECIP*CAYSQ*H1*A
    SIG1=SIG1+DEL1
    SIG2=SIG2+DEL2
    IF(DABS(DEL1)-4.0D-16)4,3,3
  3 IF(DABS(CRIT)-DABS(A))4,2,2
  4 F=PHI+SIG1
    E=PHI+SIG2
    GO TO 8
  5 CFI=1.D0
    CFJ=1.D0
    CFL=0.D0
    CFM=0.D0
    CFN=0.D0
    SIG1=0.D0
    SIG2=0.D0
    SIG3=0.D0
    SIG4=0.D0
    N=0
    FACT1=1.0D0-CAYSQ*SINP*SINP
    FACTOR=.5D0*COSP*DSQRT(CAYSQ/FACT1)
    FACTRO=FACTOR+FACTOR
    CAYDSQ=1.0D0-CAYSQ
  6 N=N+1
    RECIP=1.0D0/FLOAT(N)
    FACTN=RECIP*(FLOAT(N)-.5D0)
    FACTM=(FLOAT(N)+.5D0)/(FLOAT(N)+1.0D0)
    FACTOR=FACTOR*FACT1
    CFI1=CFI
    CFJ1=CFJ
    CFI=CFI*FACTN
    CFJ=CFJ*FACTN*FACTN*CAYDSQ
    CFL=CFL+.5D0/(FLOAT(N)*(FLOAT(N)-.5D0))
    CFM=(CFM-FACTOR*RECIP*CFI)*FACTM*FACTM*CAYDSQ
    CFN=(CFN-FACTOR*RECIP*CFI1)*FACTN*FACTM*CAYDSQ
    DEL1=CFM-CFJ*CFL
    DEL2=CFN-(FACTN*CFL-.25D0*RECIP*RECIP)*CAYDSQ     *CFJ1
    DEL3=CFJ
    DEL4=FACTM*CFJ
    SIG1=SIG1+DEL1
    SIG2=SIG2+DEL2
```

```
      SIG3=SIG3+DEL3
      SIG4=SIG4+DEL4
      IF(DABS (DEL1)-4.0D-16)7,6,6
    7 CAYMOD=DSQRT(CAYSQ)
      FLOG1=DLOG(4.0D0/(DSQRT(FACT1)+CAYMOD*COSP))
      T1=(1.0D0+SIG3)*FLOG1+FACTRO*DLOG(.5D0+.5D0*CAYMOD*DABS (SINP))
      T2=(.5D0+SIG4)*CAYDSQ*FLOG1+1.0D0-FACTRO*(1.0D0-CAYMOD*DABS(SINP))
      F=T1+SIG1
      E=T2+SIG2
      IF(PHI.GE.0.0D0) GO TO 8
      F=-F
      E=-E
    8 RETURN
      END
```